NJC

PAPER

Cite this: *New J. Chem.*, 2018, 42, 11165

Promoting effect of ceria on the performance of NiPd/CeO_2–Al_2O_3 catalysts for the selective hydrogenation of 1,3-butadiene in the presence of 1-butene†

Franklin J. Méndez, *[ab] Laurent Piccolo, [c] Roger Solano, [de] Mimoun Aouine, [c] Yanet Villasana, [af] Julia Guerra, [g] Susana Curbelo, [g] Claudio Olivera-Fuentes [g] and Joaquín L. Brito *[ah]

Received 22nd November 2017,
Accepted 24th May 2018

DOI: 10.1039/c7nj04558a

rsc.li/njc

The removal of traces of highly unsaturated compounds, such as 1,3-butadiene, from olefin feedstocks *via* selective hydrogenation is of particular importance because the oligomerization of these impurities produces deactivation and an increased pressure drop across the catalytic beds used in the polymerization processes. The present work focuses on the selective hydrogenation of 1,3-butadiene in the presence of 1-butene using ($x$$CeO_2$-)$Al_2O_3$-supported NiPd catalysts (x = 0, 1, 2, and 3 wt% CeO_2) in both liquid and gas conditions. The samples were characterized by XRD, N_2 physisorption, Zeta potential, H_2-TPR, NH_3-TPD, HRTEM and STEM-HAADF. Modifying the catalysts with CeO_2 resulted in an increase of 1,3-butadiene conversion, an enhancement of 1-butene selectivity and a decrease of butane production under liquid phase conditions. In contrast, in the gas phase both the Ce-modified and unmodified catalysts behaved similarly: while the fresh catalysts showed similar reactivity to that found in liquid phase conditions, the reacted and thermally pretreated catalysts showed increased reactivity, leading to full hydrogenation up to butane. The improvements observed under liquid phase conditions may be related to modification of the acid strength with increasing CeO_2 loading, which would increase the adsorption of 1,3-butadiene and diminish the further hydrogenation of 1-butene. Optimal activity and selectivity were observed for the catalyst with an Ni/Pd atomic ratio of 1, and loadings of 0.5 wt% Pd and 3.0 wt% CeO_2.

1 Introduction

C4 olefin-rich cuts produced by cracking reactions are purified by selective hydrogenation of trace amounts of highly unsaturated impurities using Al_2O_3-supported Pd catalysts.[1] This is necessary because removal of such impurities by other separation processes, *e.g.*, distillation, is not economically feasible due to the similar volatilities of the species in the mixture.[2] In particular, selective hydrogenation of 1,3-butadiene (BD) in the presence of 1-butene (BE) is very important since this olefin is used industrially as a co-monomer in the production of linear-low-density polyethylene.[1,3] The presence of highly unsaturated hydrocarbons leads to undesired side reactions affecting polymer quality, deactivation of the catalysts and build-up of contaminant deposits.

The monometallic Pd catalyst shows good activity for the selective hydrogenation of BD. Nevertheless, it has some limitations, *e.g.*, low selectivity to BE at high conversion of BD and a tendency to poison active sites. Addition of a co-metal is an efficient way to improve the catalytic properties of this catalyst, in particular, the selectivity to the desired alkene. The performance of Pd-based catalysts using Cu, Co, Tl, Fe, Ag, Au, Sn, Ni and Pb as co-metals has been previously reviewed by Méndez *et al.*[3] A common characteristic of all bimetallic catalysts is that the second metal decorates the Pd surface.[3]

[a] *Centro de Química, Instituto Venezolano de Investigaciones Científicas, Apartado Postal 20632, Caracas 1020-A, Venezuela*
[b] *Instituto de Física, Universidad Nacional Autónoma de México, Apartado Postal 20364, Ciudad de México 01000, Mexico. E-mail: fmendez@fisica.unam.mx, frankmendez.mz@gmail.com*
[c] *Univ Lyon, Université Claude Bernard – Lyon 1, CNRS, IRCELYON – UMR 5256, 2 Avenue Albert Einstein, F-69626 Villeurbanne Cedex, France*
[d] *Instituto de Superficies y Catálisis "Prof. Eduardo Choren", Facultad de Ingeniería, Universidad del Zulia, Maracaibo, Venezuela*
[e] *Departamento de Ingeniería Química, Grupo Catalizadores y Adsorbentes, Universidad de Antioquia - UdeA, Calle 70 No. 52-21. Medellín, Colombia*
[f] *Universidad Regional Amazónica, IKIAM, Tena, Ecuador*
[g] *Departamento de Termodinámica y Fenómenos de Transferencia, Universidad Simón Bolívar, Caracas, Venezuela*
[h] *Yachay Tech University, Urcuquí 100119, Ecuador. E-mail: jbrito@yachaytech.edu.ec, joalbrito@gmail.com*

† Electronic supplementary information (ESI) available. See DOI: 10.1039/c7nj04558a

Al_2O_3-supported NiPd has received special attention due to its improved activity and selectivity properties.[4–6] In a recent work, Hou *et al.*[7] explored the effects of different oxide supports (γ-Al_2O_3, SiO_2, CeO_2, ZrO_2 and TiO_2) on Ni–Pd bimetallic catalysts for BD hydrogenation. It was found that although the type of support affected the structure of the bimetallic particles and the selectivity to BE, it had little effect on the intrinsic activity of the bimetallic catalyst. On the other hand, in our previous work,[6] we have observed that the addition of Ni to Al_2O_3-supported Pd-based catalysts suppressed butane (BA) formation and increased the recovery of BE. In the literature, some hypotheses have been proposed to explain these performances: (i) a favourable geometrical arrangement of surface atoms could occur during annealing of the Pd atom deposition on Ni(111), favouring the adsorption of the reactants during hydrogenation,[8] (ii) a strain relaxation effect of the Ni–Pd surfaces of a Pd monolayer on Ni(110) also could contribute to alkene hydrogenation,[9] and (iii) self-poisoning or competitive adsorption between butenes and oligomers.[10]

Al_2O_3 in their different crystalline phases, from the most crystalline phase (α-Al_2O_3) to large specific surface area ones (γ-Al_2O_3), are preferred supports for selective hydrogenation catalysts. It has also been reported that there is a positive effect when the Pd/Al_2O_3 catalyst is doped with rare earth elements, such as cerium.[11,12] The influence of CeO_2 and Pd addition to the Ni/Al_2O_3 catalyst on carbon deposition from CH_4 and carbon elimination as CO_2 was studied by Yang *et al.*[11] They found that both CeO_2 and Pd can decrease the carbon deposition activity while increasing the CO_2 ability for elimination of carbon deposits, improving the resistance to carbon deposition of the Ni/Al_2O_3 catalyst. Wang and Zhang showed that Ce addition to the NiPd/Al_2O_3 catalyst enhances their activity and stability in hydrogen production from hydrocarbon mixtures by partial oxidation and steam reforming.[12] However, there are few studies of Ce-containing catalytic systems for selective hydrogenation reactions.

Ceria-containing materials have come under intense scrutiny as promoters, supports and catalysts due to their redox and acid–base properties. It has been reported that Ce-addition to Al_2O_3-supported Ni or Pd catalysts could improve certain physicochemical characteristics, such as: (i) metal–support interaction: Ni–Al_2O_3[13] and Pd–CeO_2,[14–16] (ii) structural and thermal stabilities of Al_2O_3,[17–22] (iii) metal dispersion: Ni[13] and Pd,[23] (iv) metal reducibility: Ni[13] and Pd,[15,24,25] (v) oxygen storage[26] and (vi) resistance to coke deposition.[13]

Our research group has begun to explore some NiPdCe formulations for selective hydrogenation reactions.[27,28] It has been shown that Ce-incorporation (about 0.1 wt%) to the NiPd/Al_2O_3 catalyst[27] and toluene-addition to the reaction feed[28] affected metal dispersion and diolefin adsorption, respectively. Furthermore, both activity and selectivity were also improved. Given the interesting properties of CeO_2-promoted catalysts, the objective of this work is to study the effect of higher CeO_2 loadings (1–3 wt%) in NiPd/(CeO_2-)Al_2O_3 catalysts with fixed Ni and Pd contents on certain physicochemical properties and the behaviour of selective hydrogenation of BD in the presence of BE in both liquid- and gas-phase conditions, as regards reactivity, selectivity and surface stability.

2 Experimental

2.1 Support and catalyst preparation

CeO_2–Al_2O_3 was prepared through impregnation in an excess of solution. Calculated amounts of $(NH_4)_2Ce(NO_3)_6$ (Alfa Aesar) were dissolved and added onto γ-Al_2O_3 (Alfa Aesar, 167 $m^2\ g^{-1}$, cylindrical pellets of 1/8″ diameter, previously heat-treated at 120 °C for 12 h). Different concentrations of the Ce-precursor allowed CeO_2 nominal contents of 1, 2 and 3 wt% to be obtained. The CeO_2 contents were limited to this range because it has been reported that higher loadings result in the loss of textural properties (surface area and pore volume) and poorer dispersion of the supported noble metals.[21,29,30] During impregnation, the pH was adjusted at about 8.0 with NH_4OH (4 M) and maintained under stirring. The suspension was treated in a rotary evaporator at 60 °C and 60 rpm in order to remove free moisture whereas the bound moisture was eliminated at 150 °C for 12 h in N_2 (100 mL min^{-1}). Finally, it was calcined under a flow of synthetic air (100 mL min^{-1}) using a linear heating rate of 5 °C min^{-1} up to the final temperature of 500 °C, which was held for 4 h. For identification, the samples were labeled as: **A** for Al_2O_3 and ***x*CeA** for CeO_2–Al_2O_3, where *x* indicates the amount (wt%) of CeO_2.

The incorporation of Ni and Pd onto (CeO_2-)Al_2O_3, from solutions of $Ni(NO_3)_2{\cdot}6H_2O$ (Aldrich) and $Pd(NH_3)_4Cl_2{\cdot}H_2O$ (Aldrich), was carried out following a similar procedure to that used for the Ce impregnation. However, in order to obtain egg-shell profiles of the active components, the bound moisture was eliminated at 60 °C for 12 h in N_2 (100 mL min^{-1}). In this case, the samples are denoted as **NiPd/A** and **NiPd/*x*CeA**, where Pd loading = 0.5 wt%; the Ni/Pd atomic ratio = 1; and the CeO_2 loading = *x* (*x* = 1, 2 or 3 wt%).

2.2 Physicochemical characterization

2.2.1 Crystalline phase identification. X-ray diffraction (XRD) patterns were obtained with a Siemens D-5005 diffractometer using Cu-Kα radiation (λ = 1.5456 Å), a Ni filter and a step rate of 0.02° s^{-1}. The powdered samples obtained by crushing of pellets were top loaded into 2.5 cm diameter circular cavity holders before data collection. Phase identification was made using the JCPDS library.[31]

2.2.2 Textural characteristics. Surface area and porosity were measured with a Micromeritics ASAP 2010 automatic analyzer at liquid N_2 temperature. Prior to the experiments, about 100 mg of samples were degassed overnight under vacuum at 60 °C.

2.2.3 Zeta potential. 20 mg of the sample was dispersed in an aqueous solution of NaCl (0.001 M) under ultrasonic irradiation at 35 MHz (Bandelin Sonorex Digital 10P) in an ice–water bath for 1 h. The pH of the suspensions was adjusted with either CH_3COOH or NH_4OH to 2, 4, 6, 8, 10 and 12 and then placed overnight in a Reax Heidolph 20/18 stirrer. Finally, pH and electric potential were measured using a Malvern Instruments LTD Zetasizer Nano Z 2000 instrument.

2.2.4 Elemental mapping. The selected catalyst was analyzed in two forms: (i) pellets cut transversely and (ii) ground into a powder. About 10 mg of the ground sample or 1/2 a pellet was fixed with conductive tabs onto Al-stubs and coated with a carbon layer to improve electron conduction. Finally, elemental mapping measurements were carried out using a field emission scanning electron microscope (FE-SEM FEI Inspect F50) coupled to an elemental analyzer (EDAX Apollo X-SDD).

2.2.5 Reducibility. Temperature-programmed reduction profiles in hydrogen (H_2-TPR) were obtained in a homemade system using a tubular reactor and stainless-steel capillary tubing coupled to a TCD. About 20 mg of the unreduced sample was placed in a U-shaped quartz reactor using a glass wool plug as support, heated up to 120 °C in Ar flow for 2 h and then cooled down to room temperature. The gas flow was changed to a 5% H_2 in Ar mixture and the temperature was increased to 500 °C, at a heating rate of 10 °C min^{-1}. The water desorbed during the reduction treatment was collected in a molecular sieve trap and the temperature and H_2 consumption were registered at 6 s intervals.

2.2.6 Surface acidity. Temperature-programmed desorption profiles of ammonia (NH_3-TPD) were obtained with a Micromeritics AutoChem II 2920 automatic analyser. About 20 mg of unreduced sample was charged in a U-tube quartz reactor using a glass wool plug as support and dried at 120 °C for 2 h in Ar flow. Then, the solid was cooled to 40 °C and pulses of NH_3/Ar (0.3 vol% NH_3) were injected until saturation. The sample was purged with He and the desorption process was carried out from 40 to 500 °C with a temperature ramp of 10 °C min^{-1}. The ammonia desorbed was detected by a TCD.

2.2.7 Nano- and micro-structure. The internal structure of two selected samples were examined by high-resolution transmission electron microscopy (HRTEM) and scanning-transmission electron microscopy in the high-angle-annular-dark-field mode (STEM-HAADF) using a FEI Titan G2 Cs aberration-corrected ETEM (in high-vacuum mode) operated at 300 kV and coupled to an energy-dispersive X-ray (EDX Oxford X-Max) elemental analyser. About 5 mg of the powdered samples obtained from several crushed pellets were dispersed in ethanol before dropping the suspension onto a carbon-covered copper grid, followed by drying. A standard reducing pretreatment at atmospheric pressure was applied. The temperature was increased at a linear rate of 3 °C min^{-1} up to 300 °C, which was held for 2 h under pure H_2 flow (60 mL min^{-1}).

2.3 Catalytic performance

A reactivity study of NiPd/(CeO_2-)Al_2O_3 catalysts in the selective hydrogenation of BD in the presence of BE was conducted in two different reaction systems, under the conditions described below.

2.3.1 Liquid-phase reactions. These measurements were carried out in a total recirculation system with an external fixed-bed reactor under the following reaction conditions: temperature, T = 40 °C; total pressure, P = 1.38 MPa; and weight hourly space velocity, WHSV = 120 h^{-1}. This reaction system consists of the circulation of the liquid mixture over a catalytic bed coupled to an analysis system with negligible loss of volume.

In a typical experiment under liquid-phase condition, the fresh catalyst in pellet form (~1 g) was pre-reduced *ex situ* under H_2 (WHSV = 12 000 h^{-1}) in a fixed-bed reactor (U-shaped Pyrex® tube, 200 mm in length and 17 mm in internal diameter). The temperature was increased at a linear rate of 3 °C min^{-1} from room temperature to a final temperature of 300 °C, which was held for 2 h. After pretreatment, the sample was cooled to room temperature in H_2 and immersed in anhydrous heptane to prevent re-oxidation.

A fixed-bed reactor (stainless-steel 316 tube with a length of 110 mm and an internal diameter of 17 mm) packed in three sections separated with glass wool plugs (L1 = L3 = glass microspheres and L2 = catalyst) was connected to the reaction system. The catalyst surface was refreshed using a flow of 30 mL min^{-1} of H_2 for 30 min at the reaction temperature. The stirred vessel was fed with BE, BD and H_2 as reactants, hexane (HX) as solvent and pentane (PA) as internal standard, with a composition of HX : PA : unsaturated compounds of 73 : 2 : 25 by volume and a molar ratio of BE : BD of 20 : 1. The reaction was started by pressurizing with H_2 and recirculating the liquid/gas mixture by means of a high-pressure pump.

The effluent stream from the reactor was analyzed using an on-line gas chromatograph (Agilent Technologies model GC 6890) equipped with a flame ionization detector (FID) and a GS-Gaspro capillary column (60 m length and 0.32 mm internal diameter). The chromatograms were integrated by the ChemStation Plus software and converted to mass and mole percentages as recommended by Huang *et al.*[32]

2.3.2 Gas-phase reactions. These measurements were carried out in a stainless-steel static reactor usually devoted to low-surface-area samples. This reaction system consists of an ultra-high vacuum (UHV) setup, which was used here for sample heating, coupled to a reaction and analysis system, as has been previously reported.[33]

In a typical experiment under gas-phase conditions, the fresh catalyst (~4 mg, as powdered samples obtained from crushed pellets of the catalysts) was placed in the reaction cell. A mixture of ultrapure gases based on BD (0.1 mbar), BE (2.0 mbar), H_2 (2.0 mbar) and Ar (4.0 mbar), previously prepared in a separate chamber, was injected into the reactor. This procedure allowed the same molar ratio BE/BD = 20 that was utilized for the liquid-phase reactions to be kept. In some experiments, the sample was heated under UHV between 25 and 400 °C, prior to catalytic measurements.

During the reaction, the reactive mixture was continuously sampled and analyzed by a mass spectrometer (MS). The signal intensities at m/z = 2, 40, 54, 56 and 58, which correspond to the masses of H_2, Ar (internal calibration standard), BD, butenes (BEs) and butane (BA), respectively, were monitored. In order to discriminate among the three BEs isomers, gas sampling was simultaneously performed every 10 min for on-line analysis by gas chromatography using an Agilent Technologies GC-6850 with an FID detector and a HP-AL/KCl capillary column. At the end of the first reaction run, the products were evacuated, and the reaction–evacuation cycle was repeated to assess the catalyst stability. Reaction tests were run for up to 120 min.

3 Results and discussion

3.1 Material characterization

XRD patterns of the unmodified and the CeO_2-modified Al_2O_3 and their comparison with the diffractogram of a CeO_2 sample obtained under similar synthesis conditions are shown in Fig. 1. All the samples presented three peaks at 39.4°(222), 46.1°(400) and 67.1°(440)/2θ corresponding to γ-Al_2O_3 (JCPDS card number 10-0425).[31] The sample with 1 wt% ceria loading did not show any diffraction signals corresponding to CeO_2. This is ascribed to the small crystallite size and/or the small amount of ceria. On the other hand, the samples with 2 and 3 wt% ceria loading presented four visible although small peaks at 28.5°(111), 33.1°(200), 47.5°(220) and 56.3°(311)/2θ and two weak contributions at 76.7°(331) and 79.1°(420)/2θ assigned to cubic CeO_2 (JCPDS card number 81-0792),[31] maintaining the diffraction maxima and, therefore, the crystal structure of γ-Al_2O_3. The XRD patterns of the catalysts did not show any additional diffraction signal corresponding to metal or metal oxide phases, such as Ni, NiO, Pd, PdO, Ni_xPd_y (see ESI,† Fig. S1). This could be ascribed to the small crystallite size or low metal content of the metal oxide components over the support.

Nitrogen physisorption isotherms of the supports were classified as Type IV with a hysteresis loop of Type H2 (see ESI,† Fig. S2a). This is attributed to mesoporous materials and a hysteresis loop of this kind is characteristic of spheroidal cavities, voids between closely packed spherical particles or ink-bottle-shaped pores.[34,35] The hysteresis loop ends at high values of relative pressure (P/P_0 = 0.6–0.7), which also suggests the presence of a large number of large pores (meso- and/or small macropores). This result was corroborated by the pore size distributions (see ESI,† inset of Fig. S2a) and the average pore diameter values at about 7 ± 1 nm (Table 1).

The specific surface area values of alumina appear to increase with the presence of CeO_2 (Table 1). Some authors have reported that low CeO_2 loadings could stabilize the Al_2O_3 surface.[17–22] Damyanova *et al.*[21] prepared the CeO_2–Al_2O_3 similarly to us (impregnation method), and assumed that this increase of the specific surface area is due to prevention of the thermal transformation of γ-Al_2O_3 to other phases (*e.g.*, δ, θ, α) of lower surface area. Although it is clear that CeO_2 can partially stabilize the surface area of alumina, the reference main results indicate that the extent of such stabilization depends on several factors, including loading, dispersion, temperature and atmosphere.[18] The mechanism by which this occurs is still a matter of debate in the literature but it is most likely to be related to the formation of microdomains of cerium aluminate on the alumina surface, which will lock highly reactive coordinative unsaturated Al ions into a thermally stable structure. Despite these texture changes, the PZC of the supports did not change significantly (±0.1) with increasing CeO_2 loading. These PZC values are consistent with previous reports of different Al_2O_3 obtained by other preparation methods (PZC ~ 7.8).[36–38]

Table 1 Physicochemical characteristics of the supports and catalysts

Samples	S_{BET}[a] ($m^2\ g^{-1}$)	V_p[b] ($cm^3\ g^{-1}$)	D_p[c] (nm)	Zeta potential (PZC)
A	167	0.50	7	7.8
1CeA	189	0.56	7	7.9
2CeA	197	0.60	7	7.8
3CeA	181	0.54	7	7.7
NiPd/A	146	0.47	7	—
NiPd/1CeA	115	0.48	8	—
NiPd/2CeA	102	0.32	7	—
NiPd/3CeA	103	0.31	7	—

[a] Specific surface area determined by the Brunauer–Emmett–Teller method. [b] Pore volume obtained at a relative pressure of 0.99. [c] Mean pore diameter determined from the desorption isotherms by the Barret–Joyner–Halenda method.

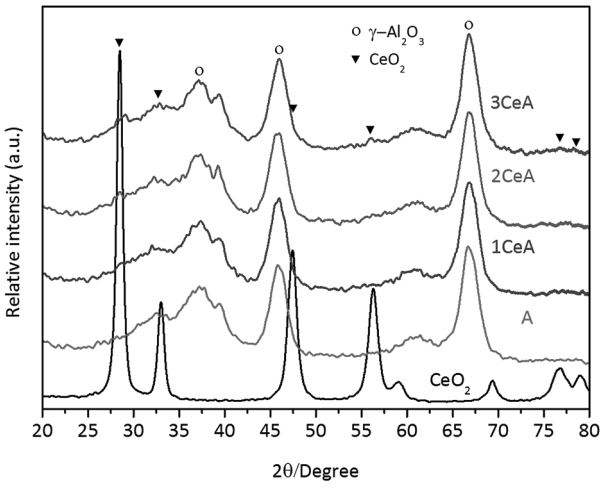

Fig. 1 X-ray diffraction patterns of the unmodified and CeO_2-modified Al_2O_3. Pure CeO_2 obtained by calcination of $(NH_4)_2Ce(NO_3)_6$ at 500 °C is also shown.

Ni and Pd simultaneous incorporation onto (CeO_2-)Al_2O_3 did not produce important modifications in the pore shapes and dimensions. This is evidenced because the N_2 physisorption isotherm and hysteresis remained unchanged after metal incorporation (see ESI,† Fig. S2b). Table 1 shows that the S_{BET} and V_p of the catalysts are always lower than those of the corresponding supports, which can be attributed to partial blockage of the pores. This negative effect was bigger for CeO_2–Al_2O_3-supported catalysts compared to their respective CeO_2-free analogues and this could be attributed to the agglomeration of some metallic particles at the external surface of the pellets. Similar results have previously been reported for analogous catalysts: Ni/CeO_2–Al_2O_3,[13] Pt/CeO_2–Al_2O_3,[39] and Pd/CeO_2–Al_2O_3.[30]

The elemental mapping of the cross section of the NiPd/3CeA catalyst in pellet form is shown in Fig. 2. It can be seen that this methodology permitted the acquisition of an egg-shell distribution of active metals and a uniform distribution of support components, *i.e.*, the Ni and Pd concentrations decrease from the edge to center and Ce, Al and O are evenly distributed over the total volume. The difference is probably caused by the drying procedures. A relatively high temperature for the removal of the bound moisture (150 °C), as is used after Ce incorporation, produces a faster drying, preventing Ce migration and causing a uniform metallic distribution. In contrast, a lower temperature (60 °C), as is used for the Ni and Pd simultaneous incorporation,

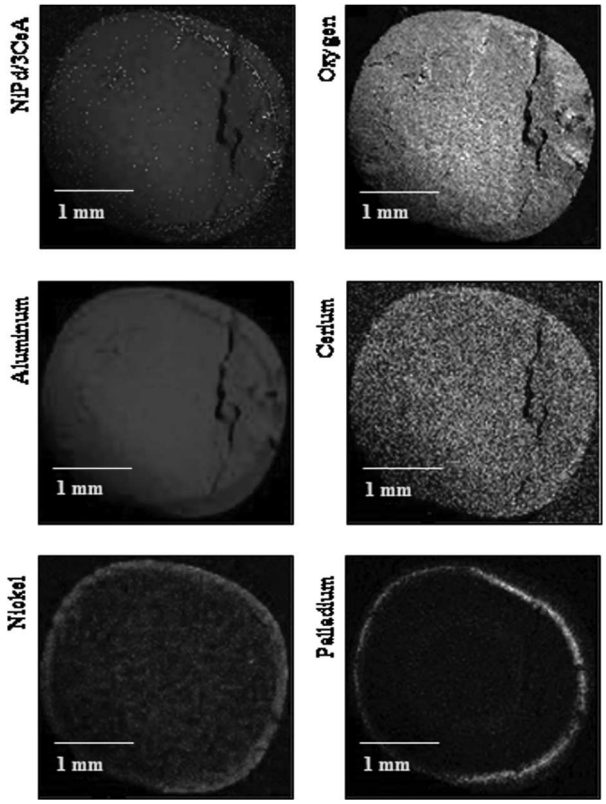

Fig. 2 Elemental distributions of a typical Ce-containing catalyst (NiPd/3CeAl) in pellet form after cross section cut.

produces metal migration together with water from the inside to the outside of the pellet. These results confirm the correlation between the synthesis conditions and the elemental distributions, as previously reported by Lekhal *et al.*[40] A comparison of the Ni and Pd elemental distributions showed greater mobility of Pd from the inside to the outside of the pellet, and a larger relative retention of Ni, which could be associated with the higher affinity of Ni to occupy certain sites in the structure of the γ-Al_2O_3, eventually leading to spinel-like phases. As previously reported by Ardiaca *et al.*,[41,42] this elemental arrangement inhibits some undesirable paths in the selective hydrogenation reactions, such as those leading to total hydrogenation.

Fig. 3 shows the H_2-TPR profiles of all the catalysts. At least three reduction peaks can be seen, *i.e.*, a broad signal between 320 and 500 °C (signal C) associated with NiO reduction to metallic Ni.[43,44] A signal below 100 °C (signal A) associated to PdO reduction to metallic Pd was also observed. Additional peaks were observed between 100 and 250 °C (signal B), which could be associated with Ni–Pd interaction phases.[45] On the other hand, it can be seen that CeO_2 incorporation causes a significant change in the H_2-TPR profiles, as a decrease in the reduction temperature for the ~400 °C peak (signal C), which suggests a diminution of the NiO–support interaction strength. Similar results have previously been reported by Galiasso-Tailleur *et al.*[45] However, the observed reduction temperature was slightly higher in the catalysts prepared in this work, probably because of the different pH used in the synthesis.

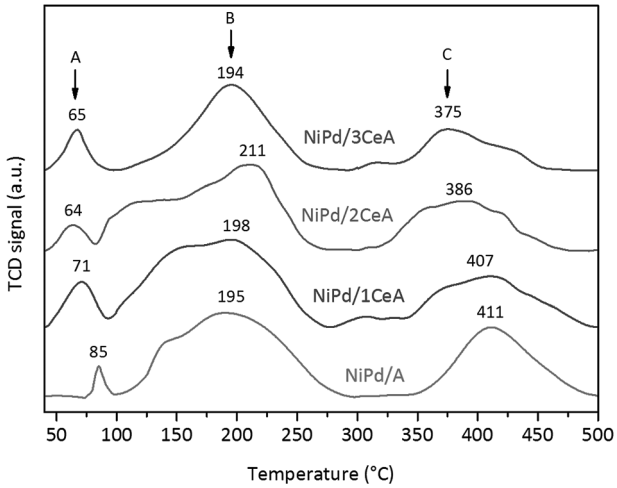

Fig. 3 H_2-TPR plots of the (CeO_2-)Al_2O_3-supported NiPd catalysts.

NH_3-TPD profiles of (CeO_2-)Al_2O_3-supported NiPd catalysts and their corresponding quantitative data as a specific surface area function are displayed in Fig. 4 and Table S1 (ESI†), respectively. The NH_3-TPR technique can provide information on the total number of acid sites without distinguishing between Brønsted and Lewis acid sites. The amount of ammonia desorbed is taken as a measurement of the number of acid centers, while the temperature ranges at which the ammonia molecules are desorbed are indicative of the strength of the sites.

The ammonia thermodesorption results show that the profile shapes of Ce-modified NiPd catalysts are very similar to that of the Al_2O_3-supported one (Fig. 4). Two signals in the low temperature region (zone I: up to 300 °C) can be seen that are attributed to desorption of NH_3 from weak and medium strength acid sites. An additional signal in the high-temperature region (zone II: between 300 and 500 °C) is also observed and is attributed to NH_3 desorption from stronger acid sites. The temperatures at the maxima of the signals in both the lower (zone I) and higher (zone II) acid strength

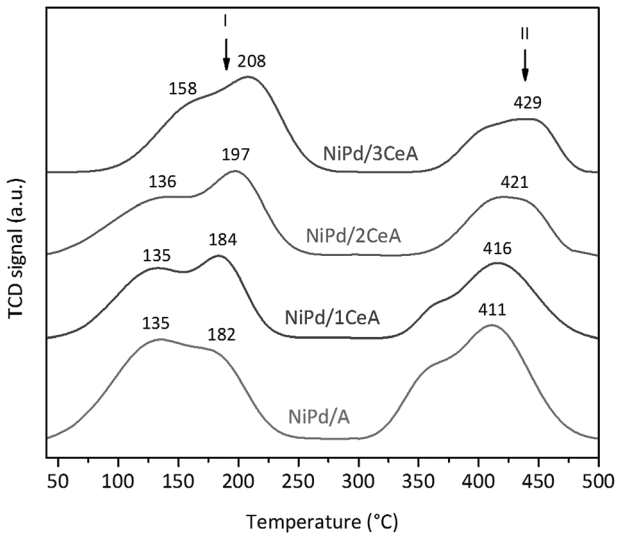

Fig. 4 NH_3-TPD plots of the (CeO_2-)Al_2O_3-supported NiPd catalysts.

zones increase with increasing CeO_2 loading. Conversely, it can be seen in Table S1 (ESI†) that the number of acid sites decreases as a consequence of the increase in the Ce amount. According to the obtained results, Ce-incorporation produced two different effects: (i) increase in acid strength (Fig. 4) and (ii) decrease of the total number of acid sites (Table S1, ESI†).

The micro- and nano-structures of the pre-reduced catalysts were analysed by HRTEM and STEM-HAADF, both combined with EDS images. Fig. 5 and 6 show the images for two representative NiPd/A and NiPd/3CeA samples, respectively. Two types of particles are seen in the HRTEM micrograph for the NiPd/A catalyst (Fig. 5). Some are fairly uniform bimetallic Ni–Pd nanoparticles with a size of 1–7 nm and there are some bigger Pd-rich aggregates with estimated sizes of up to 20 nm in diameter; these particles possess semispherical shapes that show some surface defects. On the other hand, the NiPd/3CeA catalyst (Fig. 6) shows some 10–20 nm aggregates containing Ni–Pd particles. The modified catalyst also exhibited some aggregates containing Ce, Pd and Ni traces, *e.g.*, the Ce/Pd atomic ratio was about 3 in the aggregate of Fig. 6 and the Pd/Ce atomic ratio was about 10 in the aggregate of Fig. S3a–d (ESI†), as well as pure CeO_2 nanoparticles or aggregates with a particle size of 2 and 5 nm as seen in Fig. S3e and f (ESI†).

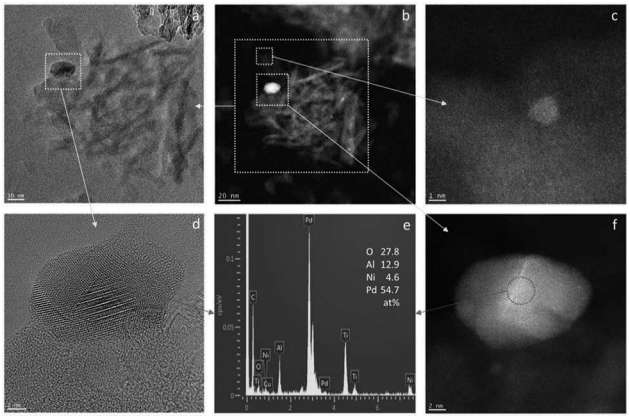

Fig. 5 HRTEM (a and d) and STEM-HAADF (b, c and f) images of the NiPd/A catalyst. The EDS spectrum in (e) shows the bimetallic nature of the observed aggregate.

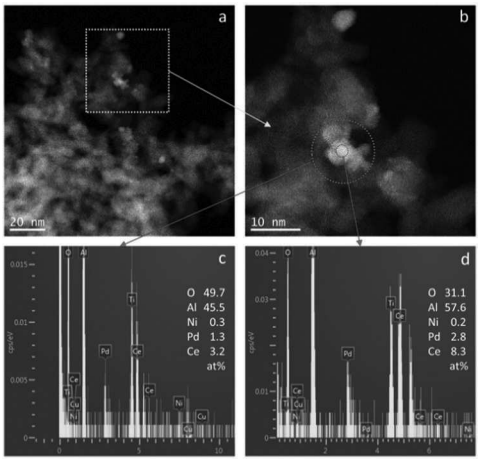

Fig. 6 STEM-HAADF images (top) and EDS spectra (bottom) of the NiPd/3CeA catalyst.

3.2 Catalytic performance

3.2.1 Selective hydrogenation of 1,3-butadiene in the liquid phase. Table 2 shows that CeO_2 incorporation increases the conversion of BD, this effect being more prominent at large reaction times. On the other hand, at low conversion ($\sim$50%), it appears that all catalysts have a similar performance. However, at high conversion ($\sim$80%), it can be seen that the yield of BE increased with 3 wt% CeO_2 loading. NiPd/A catalysts also presented low losses of BE by either isomerization to BEs or total hydrogenation to BA. In fact, with CeO_2 addition, these products were suppressed up to high conversions of BD, *e.g.*, even at a lower conversion of 50%, it can be seen that the yield towards total hydrogenation is negligible, and the yield to isomerization products is of about 0.40 mol%. The ratio between isomerization and total hydrogenation is higher for the NiPd/*x*CeA catalyst than NiPd/A, and increases with CeO_2 loading, indicating that the highest loss of BE could be due to the isomerization reactions.

The improvements observed may be related to the different trends in acidity (either total number of acid sites, Table S1, ESI;† or their relative strength, Fig. 4) with increasing CeO_2 content. Thus, BD conversion increases with increasing acid strength while the total hydrogenation to BA decreases with the decreasing number of acid sites. It is well known that selective hydrogenation depends on the ability of the partially hydrogenated products to rapidly desorb from the catalyst surface, preventing further hydrogenation reactions.[46] Nevertheless, high catalytic activity requires that the target molecules become adsorbed in the first place, which is related to the site strength, while the possibility of further hydrogenation would be diminished by a lower number of sites. On the other hand, diminished metallic phase–support interaction, as reflected by the decreasing temperature of H_2-TPR peaks upon Ce increase (Fig. 3), could result in easier reduction to the metals, improving Pd–Ni interaction and providing hydrogen to the catalyst surface. In a previous study carried out by Monteiro *et al.*[15] on the partial hydrogenation of BD in the gas phase using Pd/CeO_2–Al_2O_3 catalysts, similar improvements were observed with increased CeO_2 loading and were interpreted in terms of the Pd–Ce interaction which would modify the adsorption of BD.

3.2.2 Selective hydrogenation of 1,3-butadiene in the gas phase. In order to further investigate the stability and reactivity of the NiPd/3CeA catalyst, some additional experiments in the selective hydrogenation of BD in the presence of BE were carried out in a static reactor in the gas phase and at sub-atmospheric pressure. The evolution of hydrocarbon concentrations as a function of time is shown in Fig. 7 for two cycles of reaction/discharge. It can be seen that during cycle 1 (Fig. 7a), BD is selectively hydrogenated (*i.e.*, BE is not consumed and BA is not formed) up to the full conversion of the diene (about 40 min). Up to this point, the behaviour is similar to that found under liquid-phase conditions. BE consumption starts through isomerization to the 2-BEs and the parallel full BE hydrogenation.

Table 2 Butadiene conversion and molar composition of the out flow stream during selective hydrogenation under liquid-phase conditions

	BD conversion[a] (%)			Molar composition[b] (mol%)					Molar composition[c] (mol%)				
Catalyst	60 min	120 min	180 min	BD	BE	*c*-BE	*t*-BE	BA	BD	BE	*c*-BE	*t*-BE	BA
NiPd/A	40	63	80	2.3	97.22	0.04	0.37	0.07	1.0	97.19	0.14	1.42	0.25
NiPd/1CeA	41	70	89	2.4	97.23	0.04	0.30	0.03	0.9	94.77	0.38	3.85	0.10
NiPd/2CeA	46	77	91	2.6	97.00	0.04	0.35	0.01	0.9	97.22	0.22	1.60	0.06
NiPd/3CeAl	48	82	97	2.4	97.09	0.03	0.47	0.01	0.8	98.19	0.06	0.94	0.01

[a] At different reaction times. [b] At about 50% BD conversion. [c] At about 80% BD conversion. Reaction components: BD = 1,3-butadiene; BE = 1-butene; *t*-BE = *trans*-2-butene; *c*-BE = *cis*-2-butene; BA = butane. Reaction conditions: T = 40 °C; P = 1.38 MPa; WHSV = 120 h^{-1}.

On the other hand, it can be seen that in cycle 2 (Fig. 7b) BD consumption is much faster than in cycle 1, *i.e.*, the catalyst becomes activated during the first run. BE hydrogenation and isomerization and BA formation also occur from the start of cycle 2. This increased reactivity is possibly due to additional metal reduction, as suggested by the behavior observed after thermal pretreatments under UHV (see below). The relationship between run sequence, reactivity and selectivity in selective hydrogenation has previously been reported for catalysts based on Pd nanoparticles.[47] In contrast to reactions under liquid-phase conditions (see Table 2), the NiPd/Al (see ESI,† Fig. S4) and NiPd/3CeAl (Fig. 7) catalysts showed similar performances that indicate that the promoting effect of ceria is not observed in the gas-phase reaction. This likely is due to the fact that the egg-shell distribution of the active metals observed in the pellets is lost after grinding (see ESI,† Fig. S5), as powdered samples were used for the gas-phase experiments. Schimpf *et al.*[48] also reported that the liquid-phase hydrogenation differs from the gas-phase hydrogenation first by a lower effective diffusivity in the liquid filled pores of the catalyst. With regard to the hydrocarbon, the low diffusivity is usually compensated by a much higher concentration and consequently higher gradients of concentration. However, the Thiele modulus with regard to hydrogen is much higher in the case of liquid-phase hydrogenation because of the low diffusivity in the liquid-filled pores. The drastic fall of the hydrogen concentration towards the pellet center in this case favours selectivity towards the intermediate products. Usually the concentration of hydrogen in the liquid phase is of the same order of magnitude as in the case of gas-phase hydrogenation.

The effect of activation temperature on the catalytic performance of the NiPd/3CeA catalyst was also investigated under gas-phase conditions. The fresh catalyst was heated at 200 °C or 400 °C under UHV. This reduction pretreatment was intended to eliminate possible impurities from the surface (leftovers of the synthesis procedure) and to activate the metallic components. BEs (Fig. 8a) and BA (Fig. 8b) concentrations as a function of time were monitored by MS analysis. Fig. 8 also reports the results for the second reaction run, *i.e.* the first (fresh) and second (25 °C) runs correspond to the data of Fig. 7. These results could indicate that the UHV treatment allowed very active but less selective catalysts to be obtained. The trend in selectivity as a function of the treatment temperature is: fresh catalyst > 25 °C > 200 °C > 400 °C. The inverse trend is seen for BD conversion (not shown). Moreover, after the treatment at 400 °C, all four catalysts exhibited the same performance (see ESI,† Fig. S6). In a previous work, Piccolo *et al.*[47] deposited nanostructured ligand-free Pd particles onto an Al_2O_3 support and demonstrated that an increase in reaction rates up to a maximum performance ($<T_{max}$) can be ascribed to a certain active site contamination by adsorbed water, while a decrease of the reaction rate at higher temperatures ($>T_{max}$) can be attributed to the particle migration, aggregation and coalescence of Pd nanoparticles.

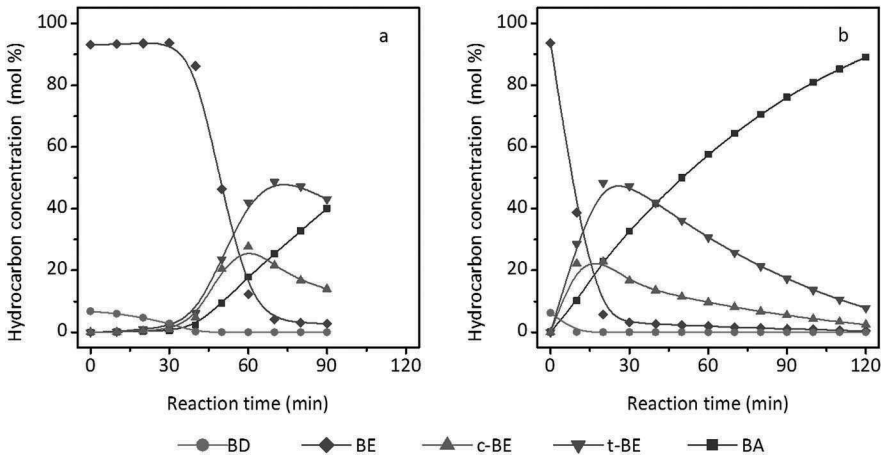

Fig. 7 Evolution of the hydrocarbon concentrations during two successive runs under gas-phase conditions using the NiPd/3CeA catalyst. (a) First run and (b) second run. Reaction components: BD = 1,3-butadiene; BE = 1-butene; *c*-BE = *cis*-2-butene; *t*-BE = *trans*-2-butene; BA = butane. Reaction conditions: T = 25 °C, initial reactant pressure = 0.1 mbar BD, 2.0 mbar BE and 2.0 mbar H_2.

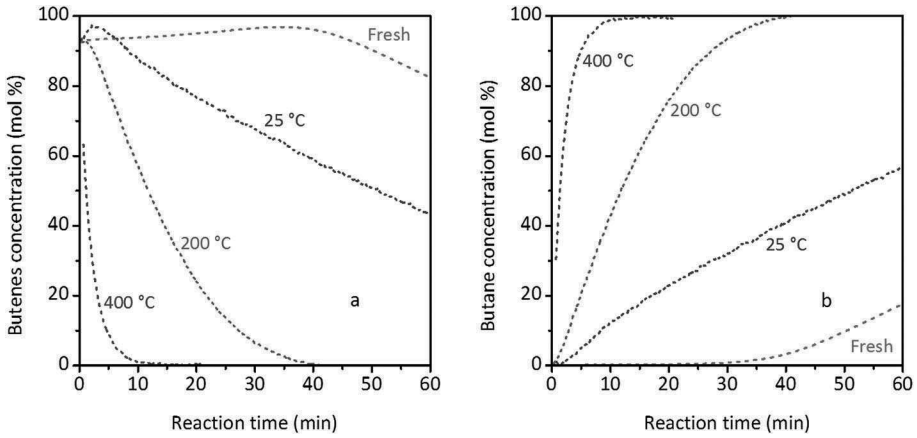

Fig. 8 Effect of activation temperature on butenes (a) and butane (b) concentration as a function of reaction time under gas-phase conditions using the NiPd/3CeA catalyst. Reaction components: BD = 1,3-butadiene; BE = 1-butene; *c*-BE = *cis*-2-butene; *t*-BE = *trans*-2-butene; BA = butane. Reaction conditions: T = 25 °C, initial reactants pressure = 0.1 mbar BD, 2.0 mbar BE and 2.0 mbar H_2.

4 Conclusions

Three mixed CeO_2/Al_2O_3 supports with 1, 2 and 3 wt% CeO_2 were employed to prepare catalysts for selective hydrogenation of 1,3-butadiene in the presence of 1-butene. The active phase components, 0.5 wt% Pd and Ni in a 1/1 atomic ratio, were distributed in egg-shell profiles, while Ce was evenly distributed through catalyst pellets. The supports and catalysts were characterized by several techniques that allowed the textural properties, acidity and reducibility of the solids to be assessed. Particularly, HRTEM and STEM-HAADF confirmed the presence of bimetallic NiPd particles in the catalysts. CeO_2–Al_2O_3-supported NiPd catalysts showed an improved performance compared to Al_2O_3-supported catalysts in the selective hydrogenation of 1,3-butadiene in the presence of 1-butene in the liquid-phase, with the best results obtained with the highest ceria loading (3 wt%). The improvements could be attributed to the variations of acidity (increased strength and decreased number of acid sites) and to modified metal precursor-support interactions upon CeO_2 incorporation. On the other hand, no effect of Ce was observed in gas-phase conditions, and an increase of activity but decrease of selectivity was found in reacted or pre-reduced catalysts. Loss of the egg-shell distribution in the samples used in the gas-phase experiments and modifications in the supported active phase could account for these results.

Conflicts of interest

The authors declare no conflict of interest.

Acknowledgements

The authors would like to acknowledge financial support by FONACIT through Project G-2005000437, as well as the technical assistance of Jelena Radosevic from UPV/EHU (Spain), and Carlos Batista and Yraida Diaz from IVIC (Venezuela). FJM personally expresses thanks to FONACIT: Science Mission Program for providing a scholarship for PhD studies.

References

1 M. L. Derrien, *Stud. Surf. Sci. Catal.*, 1986, **27**, 613–666.
2 J. A. Alves, S. P. Bressa, O. M. Martínez and G. F. Barreto, *Ind. Eng. Chem. Res.*, 2013, **52**, 5849–5861.
3 F. J. Méndez, Y. Villasana, J. Guerra, A. B. Sifontes, C. Olivera-Fuentes and J. L. Brito, *Catálisis*, 2012, **1**, 48–69.
4 R. Massard, D. Uzio, C. Thomazeau, C. Pichon, J. L. Rousset and J. C. Bertolini, *J. Catal.*, 2007, **245**, 133–143.
5 R. Hou, W. Yu, M. D. Porosoff, J. G. Chen and T. Wang, *J. Catal.*, 2014, **316**, 1–10.
6 F. J. Méndez, R. Solano, Y. Villasana, J. Guerra, S. Curbelo, M. Inojosa, C. Olivera-Fuentes and J. L. Brito, *Appl. Petrochem. Res.*, 2016, **6**, 379–387.
7 R. Hou, M. D. Porosoff, J. G. Chen and T. Wang, *Appl. Catal., A*, 2015, **490**, 17–23.
8 P. Hermann, B. Tardy, D. Simon, J. M. Guigner, B. Bigot and J. C. Bertolini, *Surf. Sci.*, 1994, **307–309**, 422–427.
9 J. S. Filhol, D. Simon and P. Sautet, *J. Am. Chem. Soc.*, 2004, **126**, 3228–3233.
10 A. Sárkány, Z. Schay, G. Stefler, L. Borkó, J. W. Hightower and L. Guczi, *Appl. Catal., A*, 1995, **124**, L181–L187.
11 Y. L. Yang, H. Y. Xu and W. Z. Li, *Acta Phys.-Chim. Sin.*, 2002, **18**, 321–325.
12 Y. H. Wang and J. C. Zhang, *Fuel*, 2005, **84**, 1926–1932.
13 S. Wang and G. Q. Lu, *Appl. Catal., B*, 1998, **19**, 267–277.
14 J. C. Summers and S. A. Ausen, *J. Catal.*, 1979, **58**, 131–143.
15 R. D. Monteiro, F. B. Noronha, L. C. Dieguez and M. Schmal, *Appl. Catal., A*, 1995, **131**, 89–106.
16 C. E. Gigola, M. S. Moreno, I. Costilla and M. D. Sánchez, *Appl. Surf. Sci.*, 2007, **254**, 325–329.
17 M. Ozawa and M. Kimura, *J. Mater. Sci. Lett.*, 1990, **9**, 291–293.
18 A. Piras, A. Trovarelli and G. Dolcetti, *Appl. Catal., B*, 2000, **28**, L77–L81.
19 S. Rossignol and C. Kappenstein, *Int. J. Inorg. Mater.*, 2001, **3**, 51–58.
20 A. Vazquez, T. Lopez, R. Gomez and X. Bokhimi, *J. Mol. Catal. A: Chem.*, 2001, **167**, 91–99.

21 S. Damyanova, C. A. Perez, M. Schmal and J. M. C. Bueno, *Appl. Catal., A*, 2002, **234**, 271–282.
22 F. A. Silva, D. S. Martinez, J. A. C. Ruiz, L. V. Mattos, C. E. Hori and F. B. Noronha, *Appl. Catal., A*, 2008, **335**, 145–152.
23 J. Luc Duplan and H. Praliaud, *Appl. Catal.*, 1990, **67**, 325–335.
24 F. L. Normand, P. Bernhardt, L. Hilaire, K. Kili, G. Krill and G. Maire, *Stud. Surf. Sci. Catal.*, 1987, **30**, 221–227.
25 F. L. Normand, L. Hilaire, K. Kili, G. Krill and G. Maire, *J. Phys. Chem.*, 1988, **92**, 2561–2568.
26 A. Holmgren, B. Andersson and D. Duprez, *Appl. Catal., B*, 1999, **22**, 215–230.
27 L. Lozano, J. Guerra, S. Curbelo, J. L. Brito and C. Olivera-Fuentes, *Chem. Eng. Trans.*, 2011, **24**, 55–60.
28 L. Lozano, J. L. Brito, C. Olivera, J. Guerra and S. Curbelo, *Fuel*, 2013, **110**, 76–82.
29 A. C. S. F. Santos, S. Damyanova, G. N. R. Teixeira, L. V. Mattos, F. B. Noronha, F. B. Passos and J. M. C. Bueno, *Appl. Catal., A*, 2005, **290**, 123–132.
30 L. S. F. Feio, C. E. Hori, S. Damyanova, F. B. Noronha, W. H. Cassinelli, C. M. P. Marques and J. M. C. Bueno, *Appl. Catal., A*, 2007, **316**, 107–116.
31 International Center for Diffraction Data, PCPDFWIN v.2.02. PDF-2 Data Base, Newtown Philadelphia, 1995.
32 Y. Huang, Q. Ou and W. Yu, *Anal. Chem.*, 1990, **62**, 2063–2064.
33 F. Morfin and L. Piccolo, *Rev. Sci. Instrum.*, 2013, **84**, 094101.
34 G. Leofanti, M. Padovan, G. Tozzola and B. Venturelli, *Catal. Today*, 1998, **41**, 207–219.
35 M. Thommes, K. Kaneko, V. Neimark Alexander, P. Olivier James, F. Rodriguez-Reinoso, J. Rouquerol and S.W. Sing Kenneth, *Pure Appl. Chem.*, 2015, **87**, 1051–1069.
36 C. P. Huang and W. Stumm, *J. Colloid Interface Sci.*, 1973, **43**, 409–420.
37 R. Sprycha, *J. Colloid Interface Sci.*, 1989, **127**, 1–11.
38 M. Farooq, A. Ramli and D. Subbarao, *J. Chem. Eng. Data*, 2012, **57**, 26–32.
39 S. Damyanova and J. M. C. Bueno, *Appl. Catal., A*, 2003, **253**, 135–150.
40 A. Lekhal, B. J. Glasser and J. G. Khinast, *Chem. Eng. Sci.*, 2004, **59**, 1063–1077.
41 N. O. Ardiaca, S. P. Bressa, J. A. Alves, O. M. Martínez and G. F. Barreto, *Catal. Today*, 2001, **64**, 205–215.
42 N. O. Ardiaca, S. P. Bressa, J. A. Alves, O. M. Martínez and G. F. Barreto, *Stud. Surf. Sci. Catal.*, 2001, **133**, 527–534.
43 S. L. Chen, H. L. Zhang, J. Hu, C. Contescu and J. A. Schwarz, *Appl. Catal.*, 1991, **73**, 289–312.
44 B. W. Hoffer, A. Dick van Langeveld, J. P. Janssens, R. L. C. Bonné, C. M. Lok and J. A. Moulijn, *J. Catal.*, 2000, **192**, 432–440.
45 R. Galiasso-Tailleur and J. Ravigli-Nascar, *Appl. Catal., A*, 2012, **439–440**, 125–134.
46 G. Gómez, P. G. Belelli, G. F. Cabeza and N. J. Castellani, *Appl. Surf. Sci.*, 2015, **353**, 820–828.
47 L. Piccolo, A. Valcarcel, M. Bausach, C. Thomazeau, D. Uzio and G. Berhault, *Phys. Chem. Chem. Phys.*, 2008, **10**, 5504–5506.
48 S. Schimpf, J. Gaube and P. Claus, in *Basic Principles in Applied Catalysis*, ed. M. Baerns, Springer, Berlin, 2004, pp. 85–123.